Methodology for Estimating the Corrosion-Induced Degradation Trajectory of 304L Stainless Steel in Nitric Acid

Abdoulaye Affadine Haoua [1], Thibaud Henin [1], Flavien Peysson[1], and Jean-Baptiste LEGER [1]

[1] *IQANTO - PREDICT, 19 Avenue Forêt de Haye, Vandoeuvre-lès-Nancy Cedex, 54519, France*

haoua.abdoulaye.affadine@predict.fr

flavien.peysson@predict.fr

jean-baptiste.leger@predict.fr

ABSTRACT

Corrosion-induced degradation is a major challenge for the integrity management of industrial equipment operating in aggressive nitric acid environments, particularly in the nuclear industry. Austenitic stainless steel 304L is widely used in such conditions due to its corrosion resistance. However, predicting its long-term degradation remains difficult because corrosion kinetics depend on multiple operating parameters (e.g., temperature, nitric acid concentration, exposure history, and oxidizing species), while available experimental data remain sparse, heterogeneous, and mostly limited to laboratory studies.

This work proposes a methodology for estimating the corrosion-induced degradation trajectory of 304L stainless steel using data extracted exclusively from the scientific literature. First, a structured database of gravimetric corrosion tests was built from published studies and standardized by converting mass losses into equivalent thickness losses under the assumption of uniform corrosion. The collected data were categorized according to exposure conditions, and only renewed nitric acid environments were retained as representative of industrial operating conditions.

Based on these data, a power-law degradation model was identified to describe thickness loss as a function of time. The parameters of this model were then estimated using machine learning approaches based on decision-tree regression, allowing the prediction of degradation parameters as functions of operating conditions such as temperature, nitric acid concentration, and environmental descriptors. Model performance was evaluated using a leave-one-out cross-validation strategy adapted to the limited dataset size.

Finally, the predicted degradation parameters were combined with operating-condition sequences in order to reconstruct cumulative degradation trajectories under variable conditions. The proposed approach provides a reproducible and physics-guided framework for estimating degradation trajectories despite limited data availability and constitutes a promising basis for prognostics and remaining useful life (RUL) assessment of equipment exposed to nitric acid environments.

Keywords: Degradation trajectory; Corrosion; 304L stainless steel; Nitric acid; Machine learning; Prognostics

1. INTRODUCTION

Nitric acid environments are widely encountered in nuclear fuel reprocessing plants, where strongly oxidizing chemical conditions prevail. In such systems, austenitic stainless steels such as 304L, 316L, and 310Nb are commonly used for the fabrication of process equipment, including tanks, piping, and heat exchangers, because of their overall corrosion resistance in nitric media (Sun et al., 2022; Fauvet, 2012; Ningshen, Kamachi Mudali, Amarendra, & Raj, 2009; Fauvet et al., 2008; Raj & Mudali, 2006; Mudali, Dayal, & Gnanamoorthy, 1993).

Among these alloys, 304L stainless steel is one of the most widely used grades for nitric acid service. This widespread use arises from a combination of practical and metallurgical advantages: (i) its low carbon content ($< 0.03\%$), which limits sensitization and carbide precipitation during welding or heat treatment; (ii) its good weldability and ease of fabrication compared with more highly alloyed stainless steels; and (iii) its lower cost and broad industrial availability (Fauvet et al., 2008; Sedriks, 1996). These characteristics make 304L particularly attractive for large-scale components operating in hot and concentrated nitric acid environments.

When exposed to nitric acid, 304L spontaneously forms a thin, self-healing passive film enriched in chromium and iron oxides that acts as an effective barrier against corro-

sion (Padhy, Paul, Kamachi Mudali, & Raj, 2011; Fauvet et al., 2008; Robin, Miserque, & Spagnol, 2008; Landolt, 2007). However, its stability may be altered under several physicochemical or operational conditions, including high temperature, elevated nitric acid concentration, the presence of strongly oxidizing species (e.g., Ce(IV), V(V), Cr(VI)), stagnant or poorly renewed media, condensate zones, or mechanical stresses near welds (Coriou, Hure, & Plante, 1961; Fallet, 2015; Balbaud, Sanchez, Fauvet, Santarini, & Picard, 2000; Schosger, 1996; Sedriks, 1996). Under such conditions, long-term material durability and corrosion resistance can be significantly reduced.

Two main degradation modes are generally reported in nitric acid environments: uniform corrosion (also referred to as generalized corrosion), which affects the entire surface homogeneously, and intergranular corrosion (IGC), which develops preferentially along grain boundaries (Gwinner et al., 2016; Sedriks, 1996). Numerous studies have shown that, under controlled and well-managed operating conditions, 304L tends to remain in the passive domain and uniform corrosion is the predominant degradation mode (Fauvet, 2012; Fauvet et al., 2008). Accordingly, **uniform corrosion is assumed in the present study**.

Estimating the long-term degradation of 304L stainless steel under uniform corrosion conditions is essential for ensuring the safe operation of critical equipment, optimizing maintenance planning, and supporting remaining useful life (RUL) assessment. However, existing approaches remain limited by the cost and duration of experimental campaigns and by empirical or simplified models that, being developed under specific conditions, do not fully capture the complexity and variability of corrosion phenomena in nitric acid environments.

The objective of this work is to propose a reproducible, physics-guided framework for estimating the corrosion-induced degradation trajectory of 304L stainless steel in nitric acid environments. The proposed approach relies on literature-derived gravimetric data, a degradation law representative of uniform corrosion kinetics, and a predictive modeling strategy enabling the reconstruction of degradation trajectories under variable operating conditions. Although the methodology has not yet been applied to a specific industrial case study, it lays the foundation for future developments aimed at anticipating corrosion-driven ageing in equipment operating under highly oxidizing nitric acid environments.

The remainder of this paper is organized as follows. Section 2 reviews existing approaches for studying, modeling, and monitoring the corrosion of 304L in nitric acid environments. Section 3 presents the proposed methodology. Section 4 discusses the results, and Section 5 presents the conclusions, recommendations, and future research directions for corrosion-related prognostics.

2. STATE-OF-ART

This section reviews current approaches used to study, model, and monitor the corrosion of 304L stainless steel in nitric acid environments, with a focus on approaches relevant to uniform corrosion.

It should be noted that a significant portion of the literature is devoted to intergranular corrosion (IGC), for which specific modeling approaches have been developed (e.g., stochastic models, cellular automata, SCIANS-type models) (Jahns et al., 2017; Gwinner et al., 2010; Bague, Chachoua, Tran, & Fauvet, 2009; Beaunier, Froment, & Vignaud, 1980). While these approaches are relevant for localized degradation, they are not directly applicable to the present study, which focuses exclusively on uniform corrosion.

2.1. Experimental and Modeling Approaches

2.1.1. Experimental Approaches

Experimental investigations constitute the primary approach used to study the corrosion behavior of 304L stainless steel in nitric acid environments. These studies typically rely on controlled laboratory experiments and can be broadly classified into three main categories:

Gravimetric (Immersion) tests

Gravimetric tests, based on the measurement of mass loss of specimens immersed in nitric acid under controlled conditions of temperature, concentration, and exposure time, constitute the most widely used method for quantifying corrosion-induced degradation of 304L stainless steel over time.

These tests are conducted over a range of nitric acid concentrations and temperatures, as well as under different solution renewal conditions (batch renewal at regular intervals, continuous renewal, or non-renewed environments). They may also include the presence of oxidizing species, such as Ce(IV), Cr(VI), or V(V), in order to investigate their influence on corrosion mechanisms. More generally, these experiments are often used within parametric studies aimed at assessing the effect of one or several environmental variables on corrosion kinetics (Balbaud et al., 2000; Schosger, 1996; Coriou et al., 1961).

Corrosion rates are typically determined according to standardized procedures, such as ASTM G1 (American Society for Testing and Materials – Standard Practice for Preparing, Cleaning, and Evaluating Corrosion Test Specimens), which defines protocols for specimen preparation, cleaning, and post-exposure evaluation (Sathe, Kain, & Chandra, 2012).

Although these tests provide reliable and reproducible estimates of material loss, they present several limitations. They require long exposure durations (ranging from several days

to several months), involve significant experimental costs (equipment and consumables). In addition, they only provide a global measure of material loss, without offering detailed insights into the underlying corrosion mechanisms.

Consequently, gravimetric tests are frequently complemented by more advanced characterization techniques, such as surface analyses, solution analyses, and electrochemical methods, in order to achieve a more comprehensive understanding of corrosion phenomena.

Surface, microstructural, and solution analyses

Advanced surface characterization techniques such as Scanning Electron Microscopy (SEM), Transmission Electron Microscopy (TEM), Energy-Dispersive X-ray Spectroscopy (EDS), X-ray Photoelectron Spectroscopy (XPS), and Scanning Electrochemical Microscopy (SECM) are widely used to investigate the morphology, composition, and evolution of passive films formed on 304L stainless steel in nitric acid environments (Tcharkhtchi-Gillard et al., 2016; Robin et al., 2008). These methods provide detailed insight into surface alterations and degradation mechanisms at the microstructural scale, complementing global assessments such as gravimetric measurements.

In parallel, solution analysis techniques such as Inductively Coupled Plasma Atomic Emission Spectroscopy (ICP-AES), Inductively Coupled Plasma Optical Emission Spectroscopy (ICP-OES), Ultraviolet–Visible (UV–Vis) spectroscopy, and ion chromatography (IC) are employed to quantify dissolved metal species (e.g., Fe, Cr, Ni ions) and to monitor the evolution of oxidizing agents in nitric acid solutions (Balbaud et al., 2000). These measurements offer valuable information on dissolution kinetics and environmental changes during corrosion processes.

Electrochemical techniques

Electrochemical techniques provide rapid and sensitive tools for investigating corrosion mechanisms, owing to their ability to deliver real-time information on electrochemical processes occurring at the metal–solution interface. They are widely used to study the behavior of 304L stainless steel in nitric acid environments, particularly with respect to passive film formation and stability, as well as dissolution kinetics.

Commonly used techniques include potentiodynamic polarization, cyclic voltammetry, chronoamperometry, and electrochemical impedance spectroscopy (EIS) (Fauvet et al., 2008). These methods enable the estimation of corrosion rates through parameters such as the corrosion current density (i_{corr}) and corrosion potential (E_{corr}), the characterization of passive film properties, and the analysis of the influence of environmental conditions such as temperature, nitric acid concentration, and the presence of oxidizing species.

2.1.2. Modeling approaches

To complement experimental studies, several modeling approaches have been proposed.

Theoretical models, based on thermodynamics and electrochemistry (Nernst equation, Pourbaix diagrams, Arrhenius law), provide a fundamental understanding of corrosion mechanisms but are generally limited to simplified, equilibrium, or isolated conditions.

Empirical models establish direct relationships between corrosion rate and environmental parameters such as temperature, nitric acid concentration, or oxidizing species content. These models, typically derived from regression analysis (e.g., linear, exponential, or power-law formulations (Fallet, 2015)), are simple to implement but valid only within the experimental domain from which they originate.

Semi-empirical models, such as Butler–Volmer or Tafel-based formulations, combine physical principles with parameter fitting. While more interpretable than purely empirical laws, they require extensive calibration and remain difficult to generalize to complex industrial nitric acid environments.

2.2. Industrial Monitoring Approaches

In industrial environments, corrosion monitoring is primarily based on non-destructive techniques such as ultrasonic thickness measurements (Zima, 2024; Chen, Bai, Guo, Zou, & Meng, 2025). This method allows periodic tracking of the thinning of equipment walls and provides a direct macroscopic assessment of material loss, making it particularly suitable for monitoring uniform corrosion.

Despite its widespread use, robustness, and industrial maturity, ultrasonic monitoring presents several limitations. Measurement uncertainties, especially those associated with the measurement chain, probe positioning, and the often challenging access to equipment operating in highly oxidizing chemical environments, can affect repeatability. The requirement to maintain fixed inspection grids imposes strict constraints on measurement procedures, and subtle or early-stage degradation cannot be detected due to the inherently macroscopic nature of the technique. Moreover, thickness measurements frequently require equipment shutdowns, which may limit monitoring frequency in practice.

Consequently, although ultrasonic testing is effective for tracking degradation, it does not provide predictive capability on its own. These limitations highlight the need for complementary predictive approaches linking observed wall-thinning to underlying process conditions.

2.3. Machine Learning Approaches for Corrosion Modeling and Prediction

In recent years, machine learning (ML) has emerged as a powerful tool for modeling complex and nonlinear systems, including corrosion phenomena. Unlike traditional approaches, ML models learn relationships directly from data without requiring explicit physical formulations.

In corrosion studies, supervised learning is the most commonly used paradigm, particularly for regression tasks such as corrosion rate prediction. Frequently used algorithms include Random Forest, Gradient Boosting (XGBoost, LightGBM), Support Vector Regression (SVR), and Artificial Neural Networks (ANN) (Fang, Cheng, Gai, Lin, & Lou, 2023; Ossai, 2019).

Machine learning has been successfully applied across a wide range of industrial domains. In the oil and gas sector, several studies have demonstrated the effectiveness of ensemble models (e.g., Random Forest, XGBoost) for predicting pipeline corrosion rates based on operational and environmental parameters (Fang et al., 2023). These models are able to capture complex nonlinear interactions while providing high predictive performance.

In civil engineering, ML approaches have been used to model corrosion in reinforced concrete structures, identifying key influencing variables such as chloride concentration, resistivity, and environmental conditions (Ji & Ye, 2023).

In marine and chloride-rich environments, ML models have been applied to predict pitting corrosion resistance and critical potentials of stainless steels, often outperforming traditional empirical indices such as PREN (Qiao et al., 2023). In the nuclear field, ML has been used for corrosion monitoring, defect detection, radionuclide transport modeling, and material degradation prediction under extreme conditions (Hu & Pfingsten, 2023).

Overall, these studies highlight the strong potential of ML for corrosion prediction, particularly in complex, multidimensional, and highly variable environments.

However, despite these advances, such approaches have not yet been applied to the case of uniform corrosion of 304L stainless steel in nitric acid environments.

2.4. Identified Research Gap

Despite extensive experimental research on the corrosion of 304L stainless steel in nitric acid environments, the available data remain dispersed, heterogeneous, and often restricted to specific laboratory conditions. At the same time, machine learning (ML) techniques have shown strong potential for corrosion prediction in various industrial sectors, but have never been applied to the case of uniform corrosion of 304L stainless steel in nitric acid using literature-derived gravimetric data. This remains a critical limitation, as corrosion behavior in nitric environments depends strongly on temperature, acid concentration, oxidizing power, and solution renewal conditions.

Addressing this gap requires: (i) consolidating scattered literature data into a structured and consistent dataset; (ii) adopting a physics-guided degradation model (here, a power-law formulation for thickness loss); (iii) using ML to estimate the parameters of this model from operating conditions; and (iv) reconstructing corrosion trajectories under variable service scenarios.

A comprehensive synthesis of all corrosion datasets extracted from the literature is provided in Annex A (Table 3). In the methodology, only data corresponding to uniform corrosion under renewed nitric acid conditions are retained for predictive modeling.

The present work therefore proposes a hybrid, physics-guided methodology in which a power-law degradation model is first identified from literature data, and its parameters are subsequently predicted using ML algorithms, ensuring consistency between data-driven predictions and the underlying physics of corrosion processes.

3. PROPOSED METHODOLOGY

The proposed methodology consists of four main steps, as illustrated in Figure 1: data collection and preparation, degradation model identification, machine learning-based parameter prediction, and degradation trajectory construction.

First, data are collected from the literature, in particular from gravimetric corrosion experiments, and subsequently preprocessed through unit standardization and scaling. In a second step, a degradation model based on a power law is identified to describe the corrosion behavior of 304L stainless steel. Then, machine learning models are employed to predict the degradation parameters α and β from the operating conditions.

Finally, the predicted parameters are used to reconstruct degradation trajectories by combining elementary degradation curves according to a given operating scenario.

3.1. Data collection and preparation

In most studies investigating the corrosion of 304L stainless steel in nitric acid environments, gravimetric test results are generally reported in the form of graphical curves rather than explicit numerical datasets (Figure 2) (Balbaud et al., 2000). Consequently, the corresponding data were extracted using digitization tools such as DigitizeIt (*DigitizeIt*, 2024) and Automeris.io (*automeris.io*, 2024).

In addition, as shown in Table 3, the units used to express mass loss vary significantly across studies (e.g., mg/dm^2,

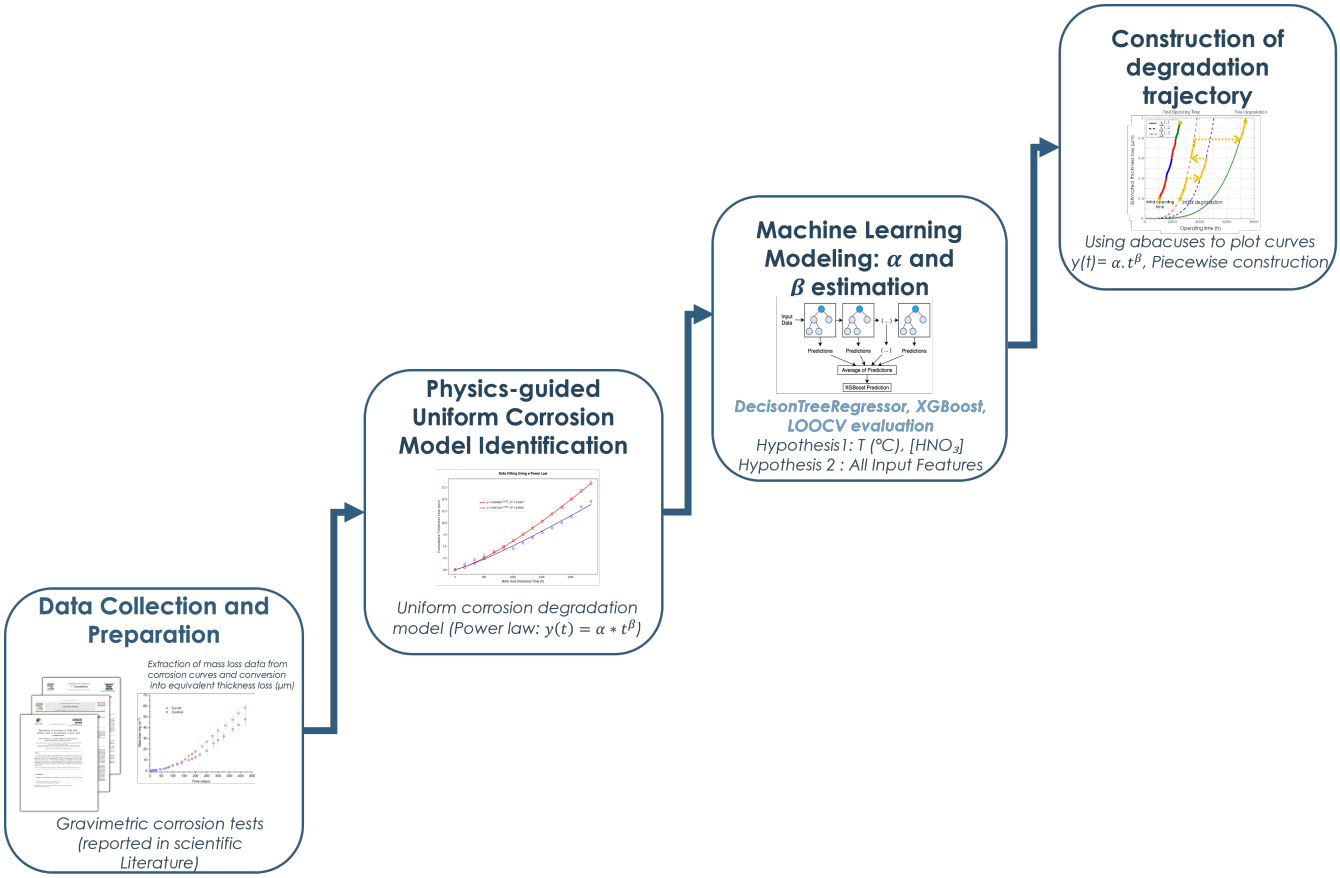

Figure 1. Overview of the proposed methodology for estimating the corrosion-induced degradation trajectory.

mg/cm^2, g/m^2, kg/m^2, or directly in μm). All data were therefore homogenized and converted into equivalent thickness loss (in μm), assuming uniform corrosion and using a density of 7.94 g/cm^3 for 304L stainless steel (Badet & Poineau, 2020; Gwinner et al., 2016).

The collected data were then categorized according to the exposure environment (see Table 3). Four main classes were identified: (i) renewed liquid environments, (ii) non-renewed liquid environments, (iii) nitric condensate environments, and (iv) alternating-phase environments involving liquid, vapor, and/or condensates. These categories are illustrated in Figure 3.

In the present study, only corrosion tests performed in renewed liquid nitric acid environments were retained. This choice is motivated by two main considerations.

First, the analysis of the collected dataset shows that gravimetric tests exhibiting predominantly uniform corrosion behavior are mainly associated with renewed liquid conditions. Since the present work assumes uniform corrosion, only datasets consistent with this assumption were selected.

Second, these experimental conditions are representative of many industrial systems where nitric acid is used. In practice, solutions are frequently renewed in order to limit the accumulation of corrosion products and highly oxidizing species that may accelerate degradation mechanisms. Furthermore, experimental studies have shown that, in certain industrial configurations, the nitric medium is continuously renewed, which contributes to maintaining predominantly uniform corrosion conditions and limits the development of localized phenomena, particularly those associated with condensates (Delwaulle, 2011; Antony, Chambrette, Junod, & Rohr, 2023).

The resulting structured and filtered dataset was then used to identify and calibrate a degradation model describing thickness loss as a function of time for 304L stainless steel in nitric acid environments.

3.2. Physics-guided Uniform Corrosion Modeling and Dataset Generation

Based on the structured and filtered dataset obtained in Section 3.1, several mathematical degradation laws were evaluated to identify a model capable of representing the uniform corrosion kinetics of 304L stainless steel in renewed

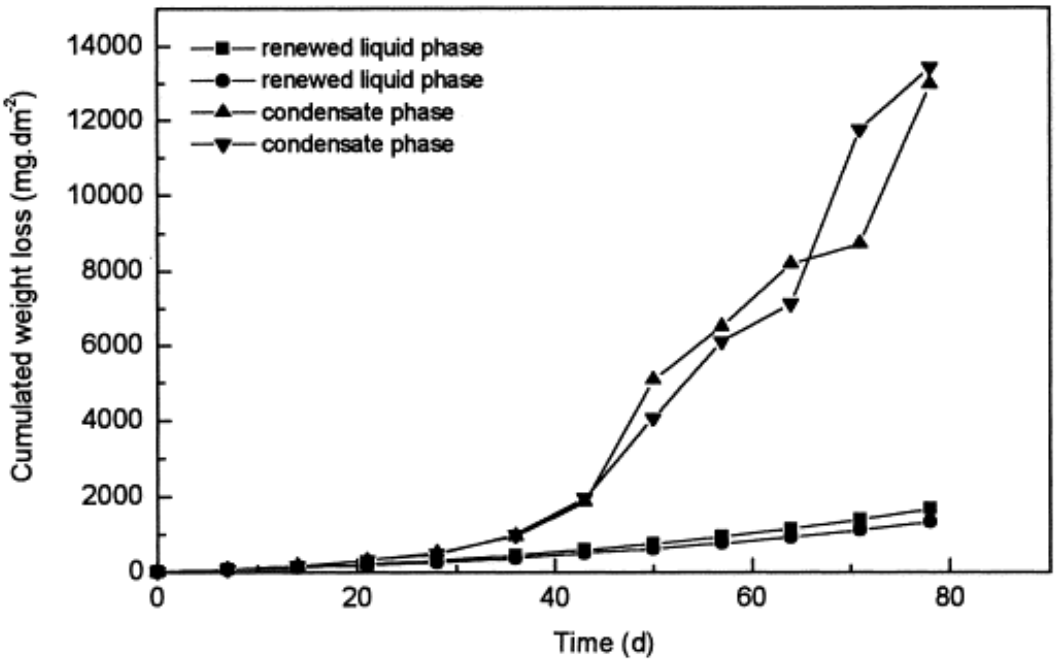

Figure 2. Illustrative evolution of cumulative mass loss due to corrosion of AISI 304L stainless steel in renewed liquid phase and in condensate phase (Balbaud et al., 2000).

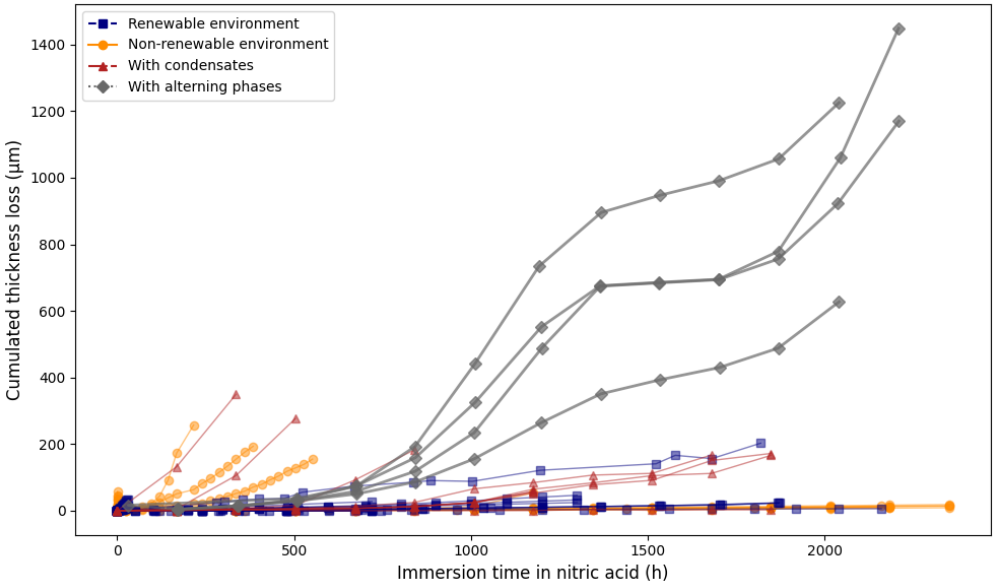

Figure 3. Cumulative thickness loss data of 304L stainless steel in nitric acid media (from the literature review), categorized by exposure medium.

liquid nitric acid environments. Among the tested formulations, the power-law relationship provided the best compromise between goodness of fit, simplicity, and consistency with the scientific literature. The retained model is expressed in Eq. (1):

$$y(t) = \alpha\, t^{\beta} \tag{1}$$

where $y(t)$ denotes the cumulative thickness loss (in μm) after an exposure time t (in hours), and α and β are model parameters that depend on the operating conditions (tempera-

ture, nitric acid concentration, oxidizing species, etc.).

Physics-guided rationale of the degradation model. Unlike purely data-driven approaches that directly predict degradation values from operating conditions, the proposed framework constrains the prediction through a predefined degradation law that is consistent with the cumulative and monotonic nature of uniform corrosion. The power-law formulation is therefore not introduced merely as an empirical fit, but as a physically consistent model commonly used to describe nonlinear corrosion kinetics under diffusion- or reaction-controlled regimes.

In this formulation, the parameter α primarily reflects the overall degradation intensity associated with the aggressiveness of the operating environment, whereas β governs the temporal evolution of corrosion kinetics. Values of $\beta > 1$ indicate accelerated degradation kinetics, while $\beta < 1$ may reflect progressive stabilization effects associated with passivation phenomena.

The role of machine learning is limited to the estimation of these physically interpretable parameters from operating conditions. The degradation trajectory itself is therefore governed by the physical model structure, ensuring consistency with known corrosion behavior. For this reason, the proposed methodology is considered physics-guided rather than purely empirical or purely data-driven.

This formulation was selected for three main reasons:

- **Established scientific relevance.** Power-law formulations are widely used to describe nonlinear degradation phenomena in various scientific fields. Melchers (Melchers, 2019) applied such formulations to long-term atmospheric corrosion, while Panchenko *et al.* (Panchenko, Marshakov, Igonin, Kovtanyuk, & Nikolaeva, 2014) demonstrated its ability to represent transitions between rapid initial corrosion and subsequent stabilization for several alloys under different climatic conditions. Similar formulations have also been reported in high-temperature oxidation environments (Ito, 1997), as well as in other degradation contexts such as mechanical wear and electrochemical aging (Han, Ouyang, Lu, & Li, 2014).
- **Physical interpretability and flexibility.** The model involves only two interpretable parameters while remaining sufficiently flexible to capture nonlinear corrosion kinetics. The parameter α is associated with the overall degradation intensity, whereas β characterizes the temporal evolution of degradation kinetics and may reflect acceleration or stabilization effects depending on environmental conditions. This balance between interpretability and descriptive capability is particularly valuable for industrial prognostics applications.
- **Strong agreement with experimental data.** Fitting the model to the collected data resulted in coefficients of determination (R^2) generally exceeding 0.9 (Figure 4), indicating strong agreement between the model and experimental measurements. These results support the suitability of the power-law formulation for representing the corrosion behavior of 304L stainless steel in renewed nitric acid environments.

Application of the power-law model and dataset generation. The parameters α and β were identified by applying a logarithmic transformation to the data and performing linear regression on the transformed variables $(\log t, \log y)$. All regressions were implemented in Python 3.10 using the `scikit-learn` library. The fitted curves are shown in Figure 4 and illustrate the strong descriptive capability of the power-law model.

For each experimental condition, the identified values of α and β were combined with the corresponding environmental descriptors (temperature, nitric acid concentration, added species, specimen preparation, renewal mode). These results are summarized in Table 1. This table constitutes the **training dataset** used for the machine learning regression models developed in Section 3.3.

3.3. Machine learning approach for predicting the degradation model parameters

The objective of this step is to estimate the parameters α and β of the power-law degradation model based on the operating conditions. To this end, two regression models based on decision trees were evaluated: `DecisionTreeRegressor` and `XGBoost`. As discussed in Section 2.3, tree-based models are widely used in corrosion modeling across various fields, including civil engineering, marine environments, and nuclear applications, due to their ability to handle limited datasets, capture nonlinear relationships, and provide interpretable structures. These properties make them suitable candidates for industrial prognostics applications where experimental data are often heterogeneous and scarce.

In this study, the models are applied to a regression task aimed at predicting the parameters α and β. The input variables, derived from the dataset structured in Section 3.2, include temperature, nitric acid concentration, solution renewal time, the presence of oxidizing species, and specimen preparation. Continuous variables were standardized using the *StandardScaler* from `scikit-learn`, while categorical variables were encoded using numerical labels. Two modeling hypotheses were considered:

- **Hypothesis H1**: Only temperature and nitric acid concentration ($[HNO_3]$) are used as input variables. This hypothesis reflects industrial constraints, as these vari-

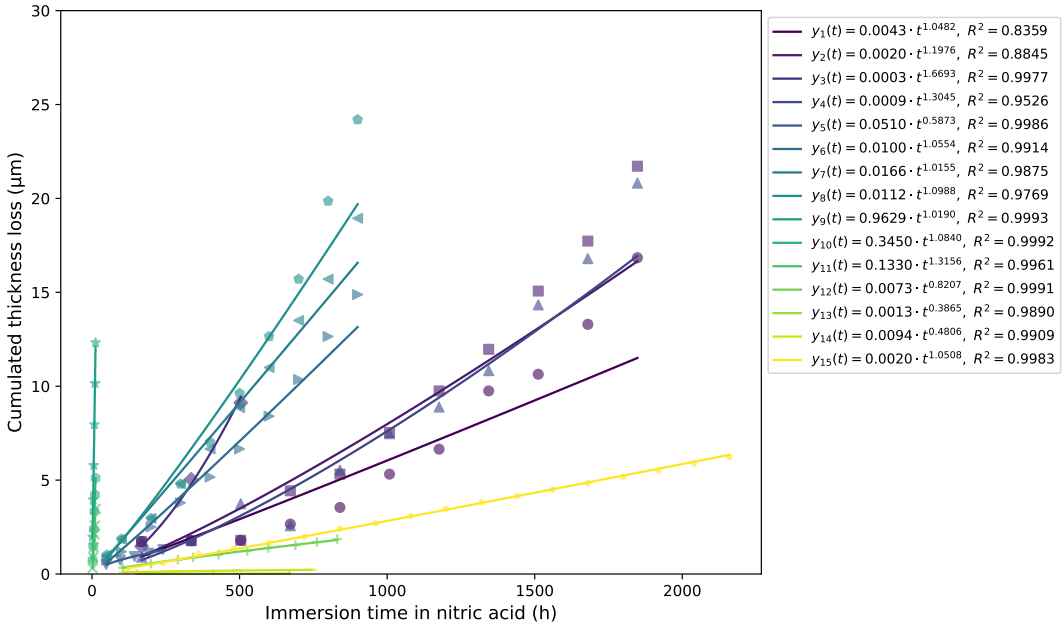

Figure 4. Power-law fitting of cumulative thickness loss of 304L stainless steel in renewed nitric acid solution (identified in blue in Figure 3).

ables are routinely measured during operation and are readily available in monitoring systems. It aims to evaluate whether the degradation model parameters can be reliably inferred from routinely monitored variables, enabling their direct use in a future PHM framework.

- **Hypothesis H2**: All available variables were used as input features, including oxidizing species, solution renewal conditions, and specimen preparation. This second hypothesis aims to evaluate the influence of additional environmental and experimental descriptors on the prediction of the degradation parameters. Although these variables are not always readily available in industrial environments due to measurement complexity, they are commonly characterized under controlled laboratory conditions and may significantly influence corrosion kinetics.

Model validation strategy. Given the limited number of available observations (15), a classical train/test split would have significantly reduced the amount of training data and increased the variability of the evaluation results. Therefore, a Leave-One-Out Cross-Validation (LOOCV) strategy was adopted to assess model generalization.

At each iteration, one observation is excluded from the training dataset and used for validation, while the remaining observations are used for model training. This procedure is repeated for all observations in the dataset. LOOCV is particularly suitable for small datasets because it maximizes the amount of data used during training while still providing an estimation of the model generalization capability and reducing the risk of overfitting.

Model performance was evaluated using the Mean Absolute Percentage Error (MAPE), defined in Eq. (2):

$$\mathrm{MAPE}(\%) = \frac{1}{n}\sum_{i=1}^{n}\left|\frac{y_i - \hat{y}_i}{y_i}\right| \times 100 \tag{2}$$

where n denotes the number of observations, y_i is the true value of observation i, and $\hat{y}_i$ is the corresponding predicted value.

Qualitative analysis of operating parameters. In addition, a qualitative feature-importance analysis was conducted in order to assess the relative influence of the operating parameters on the prediction of the degradation model parameters (α, β). Due to the limited size of the dataset and the heterogeneity of the experimental conditions collected from the literature, the resulting feature importances should be interpreted qualitatively rather than quantitatively. The objective of this analysis is therefore not to establish a strict ranking of physical influence, but rather to identify the main parameters contributing to the variability of the predicted degradation behavior.

Table 1. Dataset.

Obs.	T (°C)	[HNO_3] (mol/L)	[Added species] (mol/L)	Renewal (h)	Specimen preparation	α	β
1	111	8	None	168	Pickled and passivated	4.3×10^{-3}	1.0482
2	111	8	None	168	Pickled and passivated	2×10^{-3}	1.1976
3	111	8	None	168	Pickled and passivated	3×10^{-4}	1.6693
4	111	8	None	168	Pickled and passivated	9×10^{-4}	1.3045
5	110	9	None	48	Polished and degreased	5.1×10^{-2}	0.5873
6	110	11	None	50	Heat-treated	10^{-2}	1.0554
7	110	12	None	50	Heat-treated	1.66×10^{-2}	1.0155
8	110	13	None	50	Heat-treated	1.12×10^{-2}	1.0988
9	90	4	[Ce(IV)] = 0.01	2	Degreased + passivated	0.9629	1.0190
10	90	4	[Ce(IV)] = 0.005	2	Degreased + passivated	0.3450	1.0840
11	60	4	[Ce(IV)] = 0.005	2	Degreased + passivated	0.1330	1.3156
12	100	8	None	96	Polished and cleaned	7.3×10^{-3}	0.8207
13	30	8	None	96	Polished and cleaned	1.3×10^{-3}	0.3865
14	60	8	None	96	Polished and cleaned	9.4×10^{-3}	0.4806
15	110	7	None	120	Not specified	2×10^{-3}	1.0508

Exploration of the operating domain. To analyze the behavior of the degradation model beyond the discrete experimental conditions available in the dataset, a regular grid of temperature and nitric acid concentration was defined. This grid does not constitute a synthetic training dataset, but rather a structured exploration of the operating domain covered by the literature data. This exploration therefore remains within the interpolation domain covered by the collected literature data.

The selected ranges and discretization steps are consistent with both the experimental conditions reported in the literature and the compatibility limits of 304L stainless steel in nitric acid environments. In particular, the explored domain remains within the operating conditions commonly reported for nitric acid processes involving 304L stainless steel (Fauvet et al., 2008).

This grid-based exploration is used solely for qualitative analysis and visualization of the predicted degradation regimes, and not for model training or quantitative validation. The objective is to assess the continuity, coherence, and physical consistency of the predicted degradation parameter maps across the considered operating domain.

The explored operating domain is illustrated in Figure 5, adapted from (Fauvet et al., 2008), which summarizes the compatibility limits of stainless steels in nitric acid environments.

Detailed results are presented in Section 4.

3.4. Degradation trajectory construction

Figure 6 illustrates the overall workflow used for degradation trajectory construction.

Once the machine learning model has been trained and validated, the final step of the methodology consists in reconstructing the degradation trajectory of an equipment operating under varying conditions. This reconstruction relies on the combination of a physics-guided degradation model, expressed as a power law, and a data-driven model used to predict the parameters (α, β).

First, an operating scenario is defined. It consists of a sequence of operating modes, each characterized by a unique combination of temperature, nitric acid concentration ([HNO_3]), and an associated exposure duration. Such operating scenarios are representative of industrial nitric acid processes, where operating conditions may evolve over time depending on process phases, production campaigns, shutdown periods, or transient operating states. For instance, in nuclear fuel reprocessing applications, temperature, nitric acid concentration, and exposure duration may vary significantly according to the considered operating sequence.

To ensure consistency with the training data, the temperature and nitric acid concentration values of the scenario are normalized using the same *StandardScaler* employed during the learning phase.

For each operating mode in the scenario, the regression model predicts the corresponding degradation parameters (α, β). These parameter pairs are then used to generate elementary thickness loss curves according to the power-law model:

$$y(t) = \alpha\, t^{\beta}$$

A dedicated class, referred to as *Abacus*, has been developed to organize the predicted (α, β) values into structured maps covering the range of temperature and concentration conditions considered. These maps enable a systematic association between operating conditions and their corresponding degra-

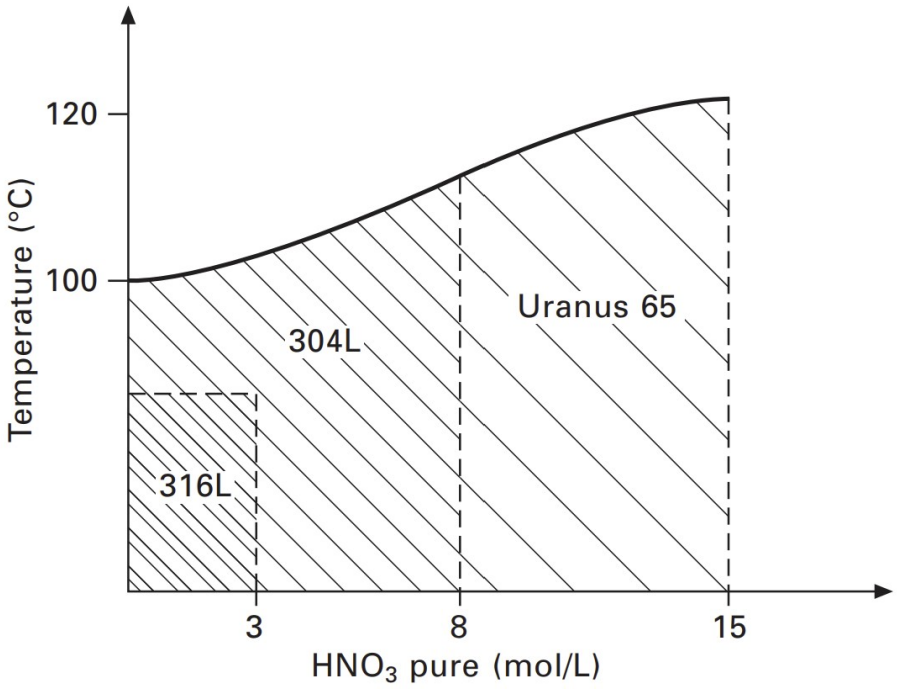

Figure 5. Illustrative operating domain of 304L stainless steel in nitric acid environments, adapted from (Fauvet et al., 2008).

dation models.

The overall degradation trajectory is then reconstructed by sequentially combining these elementary curves. Each time segment Δt contributes to a thickness loss $y(\Delta t)$ computed from the parameters associated with the corresponding operating conditions. When an initial degradation state is available, it is incorporated as an initial condition. Otherwise, the trajectory is initialized from an undamaged state ($y = 0$).

This approach enables the reconstruction of continuous and physically consistent degradation trajectories, representative of the evolution of the equipment condition under varying operating conditions. The resulting trajectory provides a continuous estimate of thickness loss over time. In an operational context, it can be compared with thickness measurements obtained through ultrasonic inspections, allowing validation and potential calibration of the model using real field data.

4. RESULTS

4.1. Model performance and cross-validation analysis

Table 2 summarizes the performance of the evaluated models under the two considered hypotheses. The reported results were obtained using a leave-one-out cross-validation (LOOCV) strategy, which provides a robust assessment of model generalization given the limited dataset size.

It can be observed that, regardless of the considered hypothesis, the `DecisionTreeRegressor` achieves higher predictive performance than `XGBoost`. This behavior can be explained by the limited number of available observations, for which decision tree models tend to better adapt to the underlying data structure, whereas ensemble methods such as XGBoost generally require larger datasets to fully exploit their generalization capabilities.

A noticeable decrease in performance is observed when moving from Hypothesis H2 to Hypothesis H1. This result indicates that temperature and nitric acid concentration alone are not sufficient to fully capture the variability of corrosion kinetics. Additional variables, such as the presence of oxidizing species and solution renewal conditions, contribute to improving the model description.

Despite this reduction in predictive performance, Hypothesis H1 remains particularly relevant from an industrial perspective, as it relies exclusively on variables that are routinely measurable and readily available during operation.

Finally, it should be noted that the parameter α exhibits relatively small numerical values, which may artificially amplify the MAPE metric for small absolute errors. Therefore, the reported MAPE values should be interpreted with caution, especially for low-magnitude degradation parameters.

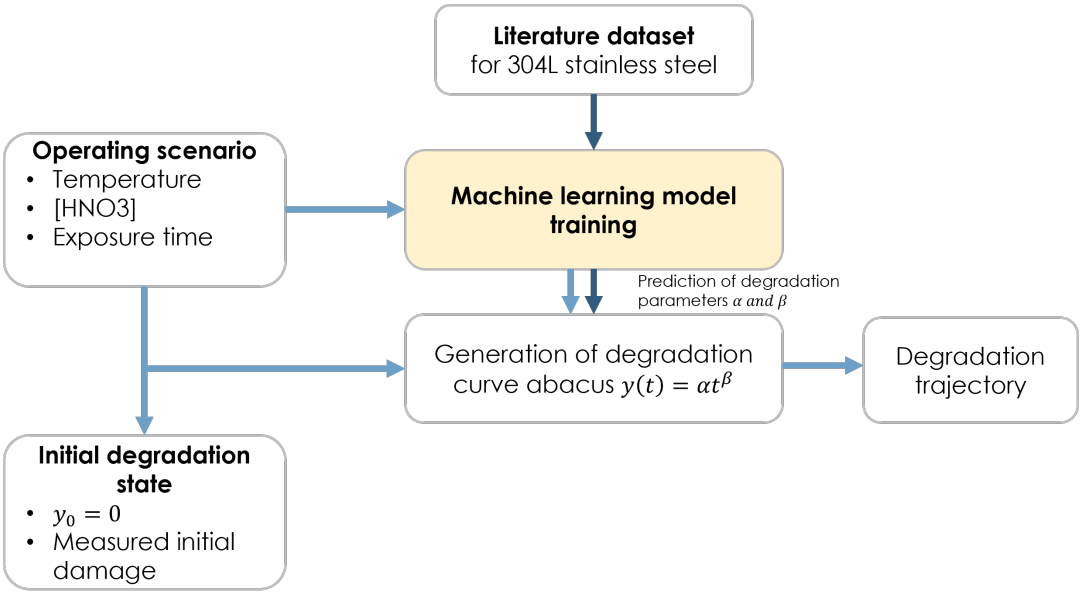

Figure 6. Overview of the degradation trajectory construction process.

4.2. Qualitative analysis of operating parameter influence

Figure 7 presents a qualitative representation of the relative influence of the main operating parameters on the prediction of the degradation model parameters (α, β). This representation is not intended to provide a strict quantitative ranking, but rather a qualitative interpretation supported by both the observed model trends and the corrosion mechanisms reported in the literature.

The analysis suggests that temperature is the dominant parameter governing corrosion kinetics, followed by oxidizing species concentration ([Ce(IV)]) and nitric acid concentration. These observations are consistent with the known behavior of stainless steels in nitric environments, where temperature strongly accelerates electrochemical and diffusion-controlled degradation mechanisms, while oxidizing species such as Ce(IV) may significantly affect passive film stability and corrosion kinetics (Fallet, 2015).

Secondary effects are associated with solution renewal conditions and specimen preparation, which may also influence local corrosion behavior and surface reactivity.

However, due to the limited number of available observations, these results should be interpreted cautiously and considered as qualitative trends rather than strict quantitative conclusions.

4.3. Degradation trajectory construction

Figure 8 presents the predicted abacuses of the degradation parameters (α, β) obtained over the regular operating-condition grid spanning temperature and nitric acid concentration.

This grid-based representation highlights the existence of distinct regions in the input space. These regions result both from the limited number of experimental configurations available in the dataset and from the intrinsic behavior of the `DecisionTreeRegressor`, which partitions the input space into subregions defined by learned thresholds.

As a consequence, the model produces piecewise constant predictions within each region, without true extrapolation capability. This behavior is consistent with the structure of tree-based models and reflects the limited coverage of the experimental dataset.

Based on these predicted abacuses, elementary degradation curves of the form $y(t) = \alpha\, t^{\beta}$ were generated for each identified region. These curves, illustrated in Figure 9, represent the corrosion kinetics associated with the different degradation regimes.

Given a time-dependent operating scenario, defined as a sequence of temperature–nitric acid concentration pairs associated with corresponding exposure durations, the elementary curves are sequentially combined in order to reconstruct the cumulative degradation trajectory.

The resulting trajectory, also illustrated in Figure 9, provides a continuous estimate of cumulative thickness loss over time while preserving continuity between successive operating conditions. These results illustrate the ability of the proposed framework to reconstruct degradation trajectories under varying operating conditions.

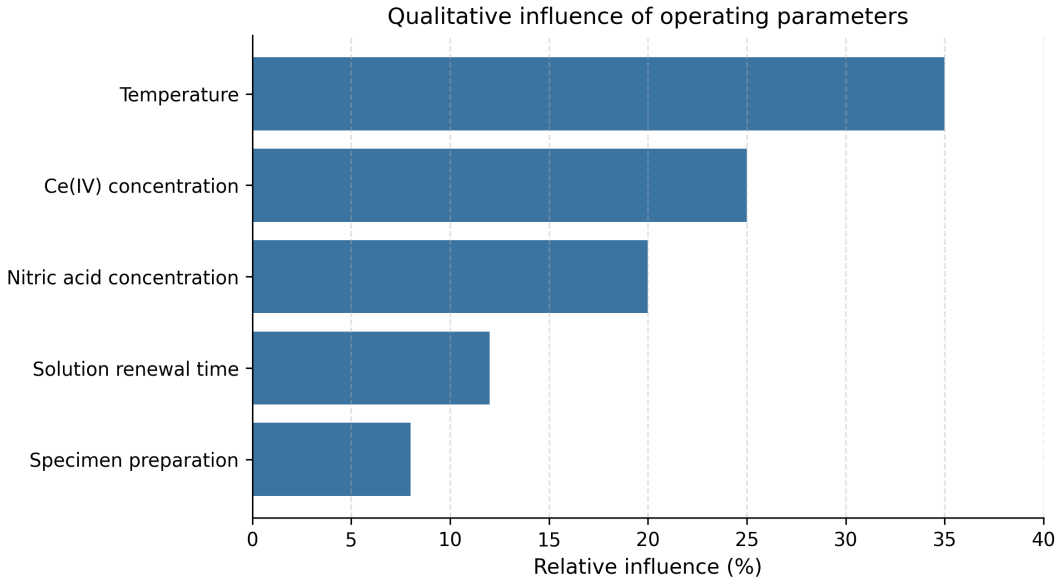

Figure 7. Qualitative influence of operating parameters on the prediction of the degradation model parameters (α, β).

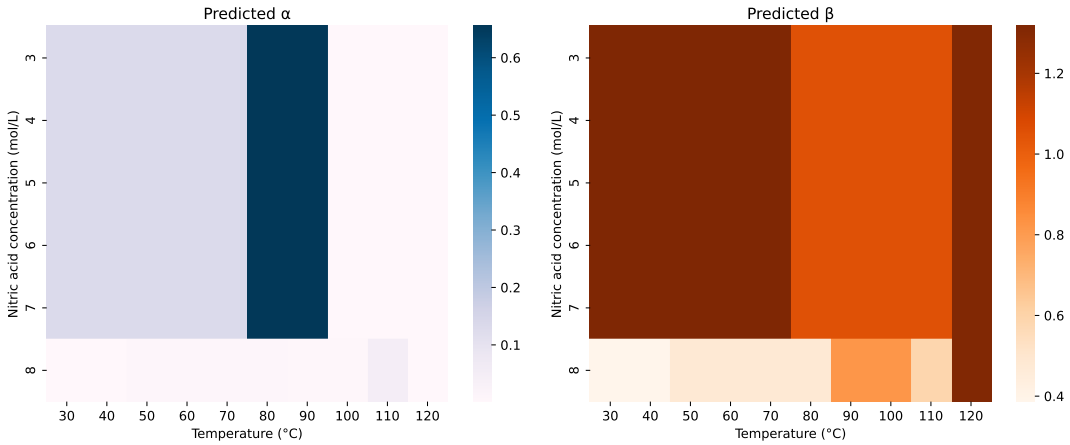

Figure 8. Overview of the predicted (α, β) abacuses over the investigated temperature–nitric acid concentration domain.

5. CONCLUSIONS AND RECOMMENDATIONS

This paper presents the development of a methodology for estimating corrosion-induced degradation of 304L stainless steel in nitric environments. The proposed hybrid approach combines data from gravimetric experiments reported in the literature, a power-law-based degradation model, and machine learning models based on decision trees.

First, a literature review was conducted to collect and structure experimental data related to the corrosion of 304L in nitric environments. These data were then preprocessed (e.g., unit standardization and scaling) to build a consistent dataset. Based on this consolidated dataset, a power-law degradation model was defined to represent the material behavior. Two regression models, DecisionTreeRegressor and XGBoost, were subsequently used to predict the degradation model parameters.

Two hypotheses were investigated: the first hypothesis is restricted to temperature and nitric acid concentration, in accordance with measurement constraints in industrial environments, while the second hypothesis includes all available input variables. The results demonstrate satisfactory predictive performance overall, although performance decreases under Hypothesis H1. Nevertheless, this hypothesis remains particularly relevant from an operational perspective due to its ease of implementation and reliance on routinely measurable variables.

Although corrosion is a complex, multi-factorial, and multi-scale phenomenon, the results demonstrate that a combined

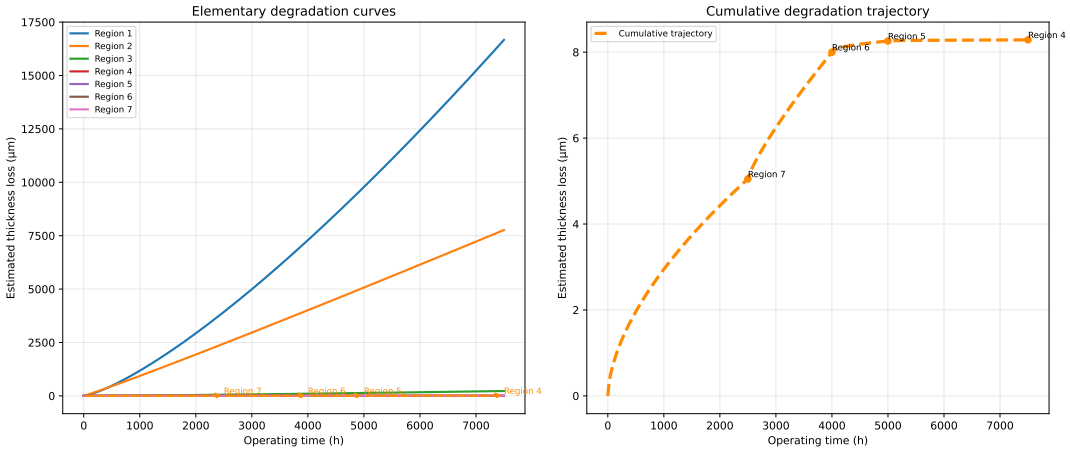

Figure 9. Elementary degradation curves and resulting cumulative degradation trajectory.

Table 2. Comparison of machine learning models and hypotheses for predicting α and β.

Model	**Hypothesis**	**Input variables**	**Output**	**MAPE (%)**
DecisionTreeRegressor	Hypothesis H1	[HNO_3] and Temperature only	α and β	**30**
DecisionTreeRegressor	Hypothesis H2	All variables	α and β	8
XGBoost	Hypothesis H1	[HNO_3] and Temperature only	α and β	38
XGBoost	Hypothesis H2	All variables	α and β	23

approach based on simplified physics-guided modeling and machine learning provides a promising pathway for degradation estimation and monitoring in nitric environments. In particular, the proposed methodology enables the construction of abacuses linking degradation parameters to operating conditions. These abacuses could serve as decision-support tools for industrial applications, allowing both the identification of operating conditions that mitigate corrosion and the estimation of the degradation state of in-service equipment.

However, the scope of this study remains limited by the small size of the available dataset (15 observations) and by the heterogeneity of the experimental conditions.

Therefore, this work should be considered as a first step toward validating the feasibility of the proposed methodology. Further improvements are required to enhance the robustness of the model and enable its deployment in industrial contexts. In particular, increasing both the quantity and quality of the training data, including data representative of real operating conditions, appears essential.

Several recommendations can be made for future work:

- enrich the dataset with experimental measurements representative of industrial environments;
- evaluate the methodology on a real use case in order to assess its applicability and, if necessary, calibrate the model;
- further develop feature selection and engineering to ensure straightforward implementation in industrial systems;
- establish a rigorous data preprocessing strategy, including balancing experimental conditions and ensuring data consistency.

DATA AVAILABILITY

Data will be made available on request.

REFERENCES

Antony, H., Chambrette, P., Junod, L., & Rohr, V. (2023, June). Pérennité des usines de la hague : retours d'expérience ≪ corrosion ≫. *Corrosion et Vieillissement*. (Accessed: 2023-07-19) doi: 10.51257/a-v1-bn3765

automeris.io. (2024). `https://automeris.io`. (Accessed: 2024-04-17)

Badet, H., & Poineau, F. (2020). Corrosion studies of stainless steel 304 l in nitric acid in the presence of uranyl nitrate: effect of temperature and nitric acid concentration. *SN Applied Sciences*, *2*(3), 1–8.

Bague, V., Chachoua, S., Tran, Q., & Fauvet, P. (2009). Determination of the long-term intergranular corrosion rate of stainless steel in concentrated nitric acid. *Journal of Nuclear Materials*, *392*(3), 396–404. doi: 10.1016/j.jnucmat.2008.12.100

Balbaud, F., Sanchez, G., Fauvet, P., Santarini, G., & Picard, G. (2000). Mechanism of corrosion of aisi 304l stainless steel in the presence of nitric acid condensates. *Corrosion Science*, *42*(10), 1685-1707.

Beaunier, L., Froment, M., & Vignaud, C. (1980). A kinetical model for the electrochemical grooving of grain boundaries. *Electrochimica Acta*, *25*, 1239–1246.

Chen, Y., Bai, X., Guo, M., Zou, F., & Meng, G. (2025). Rational determination of real-time corrosion rates based on ultrasonic wall thickness loss data. *npj Materials Degradation*, *9*, 106. doi: 10.1038/s41529-025-00660-0

Coriou, H., Hure, J., & Plante, G. (1961). Aspect electrochimique de la corrosion d'aciers inoxydables austenitiques en milieu nitrique et en presence de chrome hexavalent. *Electrochimica Acta*, *5*(1), 105-111.

Delwaulle, C. (2011). *Étude de la dissolution du dioxyde d'uranium en milieu nitrique : une nouvelle approche visant à la compréhension des mécanismes interfaciaux* (PhD thesis). Institut National Polytechnique de Lorraine, Nancy, France. (École Nationale Supérieure des Industries Chimiques, Laboratoire Réactions et Génie des Procédés)

Digitizeit. (2024). `https://www.digitizeit.xyz/fr/`. (Accessed: 2024-04-17)

Fallet, A. (2015). *Influence des ions oxydants issus de la dissolution du combustible nucléaire usé sur le comportement des matériaux de structures* (Doctoral dissertation, Université Montpellier, France). Retrieved from `https://theses.hal.science/tel-01318046` (Thèse de doctorat. NNT: 2015MONT5009)

Fang, J., Cheng, X., Gai, H., Lin, S., & Lou, H. (2023). Development of machine learning algorithms for predicting internal corrosion of crude oil and natural gas pipelines. *Computers and Chemical Engineering*, *177*, 108358. doi: 10.1016/j.compchemeng.2023.108358

Fauvet, P. (2012). 19 - corrosion issues in nuclear fuel reprocessing plants. In D. Féron (Ed.), *Nuclear corrosion science and engineering* (pp. 679–728). Woodhead Publishing. doi: 10.1533/9780857095343.5.679

Fauvet, P., Balbaud, F., Robin, R., Tran, Q.-T., Mugnier, A., & Espinoux, D. (2008). Corrosion mechanisms of austenitic stainless steels in nitric media used in reprocessing plants. *Journal of Nuclear Materials*, *375*(1), 52-64. doi: 10.1016/j.jnucmat.2007.10.017

Gwinner, B., Auroy, M., Bague, V., Chaachoua, S., Fieulaine, B., Tran, Q. T., & Tricoit, S. (2010). Corrosion intergranulaire dans l'acide nitrique des aciers inoxydables austénitiques non sensibilisés. *Revue de Métallurgie*, *107*, 441–443. doi: 10.1051/metal/2011007

Gwinner, B., Auroy, M., Balbaud-Célérier, F., Fauvet, P., Larabi-Gruet, N., Laghoutaris, P., & Robin, R. (2016). Towards a reliable determination of the intergranular corrosion rate of austenitic stainless steel in oxidizing media. *Corrosion Science*, *107*, 66–75. doi: 10.1016/j.corsci.2016.02.016

Han, X., Ouyang, M., Lu, L., & Li, J. (2014). A comparative study of commercial lithium ion battery cycle life in electric vehicle: Capacity loss estimation. *Journal of Power Sources*, *268*, 658–669. doi: 10.1016/j.jpowsour.2014.06.111

Hu, G., & Pfingsten, W. (2023). Data-driven machine learning for disposal of high-level nuclear waste: A review. *Annals of Nuclear Energy*, *180*, 109452. doi: 10.1016/j.anucene.2022.109452

Irisawa, E., & Kato, C. (2024). Estimating the corrosion rate of stainless steel r-sus304ulc in nitric acid media under concentrating operation. *Journal of Nuclear Materials*, *591*, 154914. doi: 10.1016/j.jnucmat.2024.154914

Ito, M. (1997). Time-dependent power laws in the oxidation and corrosion of metals and alloys. *Oxidation of Metals*, *48*(3-4), 213–241. doi: 10.1007/BF01046731

Jahns, K., Balinski, K., Landwehr, M., Trindade, V. B., Wübbelmann, J., & Krupp, U. (2017, 02). Modeling of intergranular oxidation by the cellular automata approach. *Oxidation of Metals*, *87*, 285–295. doi: 10.1007/s11085-017-9732-6

Ji, H., & Ye, H. (2023). Machine learning prediction of corrosion rate of steel in carbonated cementitious mortars. *Cement and Concrete Composites*, *143*, 105256. doi: 10.1016/j.cemconcomp.2023.105256

Kain, V., Shinde, S. S., & Gadiyar, H. S. (1994). Mechanism of improved corrosion resistance of type 304l stainless steel, nitric acid grade, in nitric acid environments. *Journal of Materials Engineering and Performance*, *3*(6), 699–705.

Landolt, D. (2007). *Corrosion and surface chemistry of metals*. EPFL Press.

Mayuzumi, M., Ohta, J., & Arai, T. (1998). Effects of

cold work, sensitization treatment, and the combination on corrosion behavior of stainless steels in nitric acid. *Corrosion*, *54*(4), 271–280.

Melchers, R. E. (2019). Predicting long-term corrosion of metal alloys in physical infrastructure. *npj Materials Degradation*, *3*(4), 1–17. Retrieved from https://doi.org/10.1038/s41529-018-0066-x (Open-access article) doi: 10.1038/s41529-018-0066-x

Mudali, U. K., Dayal, R. K., & Gnanamoorthy, J. B. (1993). Corrosion studies on materials of construction for spent nuclear fuel reprocessing plant equipment. *Journal of Nuclear Materials*, *203*(1), 73–82. doi: 10.1016/0022-3115(93)90432-X

Ningshen, S., Kamachi Mudali, U., Amarendra, G., & Raj, B. (2009). Corrosion assessment of nitric acid grade austenitic stainless steels. *Corrosion Science*, *51*(2), 322–329. doi: 10.1016/j.corsci.2008.09.038

Ossai, C. I. (2019). A data-driven machine learning approach for corrosion risk assessment—a comparative study. *Big Data and Cognitive Computing*, *3*(2), 28. doi: 10.3390/bdcc3020028

Padhy, N., Paul, R., Kamachi Mudali, U., & Raj, B. (2011). Morphological and compositional analysis of passive film on austenitic stainless steel in nitric acid medium. *Applied Surface Science*, *257*(11), 5088-5097. doi: 10.1016/j.apsusc.2011.01.026

Panchenko, Y. M., Marshakov, A. I., Igonin, T. N., Kovtanyuk, V. V., & Nikolaeva, L. A. (2014). Long-term forecast of corrosion mass losses of technically important metals in various world regions using a power function. *Corrosion Science*, *88*, 306–316. doi: 10.1016/j.corsci.2014.07.049

Qiao, C., Luo, H., Wang, X., Cheng, H., Bi, D., & Li, X. (2023). Machine learning-based prediction of pitting corrosion resistance in stainless steels exposed to chloride environments. *Colloids and Surfaces A: Physicochemical and Engineering Aspects*, *676*, 132274. doi: 10.1016/j.colsurfa.2023.132274

Raj, B., & Mudali, U. K. (2006). Materials development and corrosion problems in nuclear fuel reprocessing plants. *Progress in Nuclear Energy*, *48*(3), 283–314. doi: 10.1016/j.pnucene.2005.07.001

Robin, R., Miserque, F., & Spagnol, V. (2008). Correlation between composition of passive layer and corrosion behavior of high si-containing austenitic stainless steels in nitric acid. *Journal of Nuclear Materials*, *375*(1), 65-71. doi: 10.1016/j.jnucmat.2007.10.016

Sathe, S., Kain, V., & Chandra, K. (2012, 02). Corrosion behavior of type 304l stainless steels in nitric acid containing free and complexed fluoride. *Corrosion*, *68*(2), 026002-1-026002-14.

Schosger, J.-P. (1996). *Contribution à la connaissance du comportement de l'acier z3 cn 18-10 dans l'acide nitrique concentré, chaud et confiné* (Unpublished doctoral dissertation). Institut National Polytechnique de Toulouse, Toulouse, France. (Thèse de doctorat, spécialité Science des matériaux)

Sedriks, A. J. (1996). *Corrosion of stainless steels* (2nd ed.). New York: John Wiley and Sons.

Shit, G., & Ningshen, S. (2019). The corrosion behavior of compositional modified aisi type 304l stainless steel for nitric acid application. *Anti-Corrosion Methods and Materials*, *66*(2), 149–158. doi: 10.1108/ACMM-02-2018-1906

Sun, S., Zhang, L., Ma, A., Daniel, E. F., Zhang, C., & Zheng, Y. (2022). Comparison of the three-phase corrosion behavior of sin and 304l stainless steels in 6 m nitric acid solution at different temperatures. *Metals*, *12*(6), 922. doi: 10.3390/met12060922

Tcharkhtchi-Gillard, E., Benoit, M., Clavier, P., Gwinner, B., Miserque, F., & Vivier, V. (2016). Kinetics of the oxidation of stainless steel in hot and concentrated nitric acid in the passive and transpassive domains. *Corrosion Science*, *107*, 182-192.

Whillock, G. O. H., & Dunnett, B. F. (2003). Intergranular corrosion testing of austenitic stainless steels in nitric acid solutions. *BNFL Technical Report*. (Sellafield Research)

Yamamoto, T., Tsukui, S., Okamoto, S., Nagai, T., Takeuchi, M., Takeda, S., & Tanaka, Y. (1996). Gamma-ray irradiation effect on corrosion rates of stainless steel, ti and ti-5ta in boiling 9n nitric acid. *Journal of Nuclear Materials*, *228*, 162–167. doi: 10.1016/0022-3115(95)00227-8

Yamamoto, T., Tsukui, S., Okamoto, S., Nagai, T., Takeuchi, M., Takeda, S., & Tanaka, Y. (1998). Gamma-ray irradiation effects on corrosion rates of stainless steel in boiling nitric acid containing ionic additives. *Journal of Nuclear Science and Technology*, *35*(5), 353–356. doi: 10.1080/18811248.1998.9733871

Zima, B. (2024). Guided ultrasonic wave technique for corrosion monitoring and thickness variability analysis. *Measurement*, *245*, 116584. doi: 10.1016/j.measurement.2024.116584

APPENDIX A: SUMMARY OF EXPERIMENTAL DATA ON CORROSION OF 304L STAINLESS STEEL IN NITRIC ACID ENVIRONMENTS

Table 3. Summary of experimental conditions and observations from selected studies.

Reference	Material	Experimental device	[HNO_3] (mol·L^{-1})	Temperature (°C)	Exposure Time (h)	Renewal Mode	Exposure Medium	[Added Species]	Cumulated mass loss / Corrosion rate unit	Surface Preparation	Corrosion mode observed
(Sathe et al., 2012)	304L NAG Stainless Steel	ASTM A262 practice C - boiling HNO_3 immersion tests apparatus	9	Boiling (temperature values not explicitly reported)	240	Solution renewed every 48 h	Renewed liquid phase	None	Corrosion rate : mpy; mm/y	Solution-annealed; sensitized at 675°C for 1 h; water quenched	Uniform corrosion (IGC not observed)
			9	Boiling (temperature values not explicitly reported)	240	Solution renewed every 48 h	Renewed liquid phase	0.03 NaF	Corrosion rate : mpy; mm/y	Solution-annealed; sensitized at 675°C for 1 h; water quenched	Uniform corrosion (IGC not observed)
			9	Boiling (temperature values not explicitly reported)	240	Solution renewed every 48 h	Renewed liquid phase	0.03 NaF + 0.06-0.15 $Al(NO_3)_3$ (Al/NaF = 2-5)	Corrosion rate : mpy; mm/y	Solution-annealed; sensitized at 675°C for 1 h; water quenched	Uniform corrosion (IGC not observed)
			9	Boiling (temperature values not explicitly reported)	240	Solution renewed every 48 h	Renewed liquid phase	0.03 NaF + 0.50 and 1.25 $Zr(NO_3)_4$ (2× and 5× stoichiometric ratio)	Corrosion rate : mpy; mm/y	Solution-annealed; sensitized at 675°C for 1 h; water quenched	Uniform corrosion (IGC not observed)
			1	Boiling (temperature values not explicitly reported)	120	Not reported (likely non-renewed)	Non-renewed liquid phase	None	Corrosion rate : mpy; mm/y	Solution-annealed; sensitized at 675°C for 1 h; water quenched	Uniform corrosion (IGC not observed)
			1	Boiling (temperature values not explicitly reported)	120	Not reported (likely non-renewed)	Non-renewed liquid phase	0.03 NaF	Corrosion rate : mpy; mm/y	Solution-annealed; sensitized at 675°C for 1 h; water quenched	Uniform corrosion (IGC not observed)
			1	Boiling (temperature values not explicitly reported)	120	Not reported (likely non-renewed)	Non-renewed liquid phase	0.03 NaF + 0.15 $Al(NO_3)_3$ (ratio 5:1)	Corrosion rate : mpy; mm/y	Solution-annealed; sensitized at 675°C for 1 h; water quenched	Uniform corrosion (IGC not observed)
			9	Boiling (temperature values not explicitly reported)	120	Not reported (likely non-renewed)	Non-renewed liquid phase	None	Corrosion rate : mpy; mm/y	Solution-annealed; sensitized at 675°C for 1 h; water quenched	Slight IGC beginning after 120h
			9	Boiling (temperature values not explicitly reported)	120	Not reported (likely non-renewed)	Non-renewed liquid phase	0.03 NaF	Corrosion rate : mpy; mm/y	Solution-annealed; sensitized at 675°C for 1 h; water quenched	Uniform corrosion (IGC not observed)
			9	Boiling (temperature values not explicitly reported)	120	Not reported (likely non-renewed)	Non-renewed liquid phase	0.03 NaF + 0.15 $Al(NO_3)_3$ (ratio 5:1)	Corrosion rate : mpy; mm/y	Solution-annealed; sensitized at 675°C for 1 h; water quenched	Uniform corrosion (IGC not observed)
		Recirculating borosilicate glass setup	9 (initial) - varied 7.5–10.7 during boiling	Boiling (temperature values not explicitly reported)	240	Periodic renewal every 48 h (fresh solution at each period)	Renewed liquid phase	None	Corrosion rate : mpy; mm/y	Solution-annealed; sensitized at 675°C for 1 h; water quenched	Uniform corrosion (IGC not observed)
			9	Boiling (temperature values not explicitly reported)	240	Periodic renewal every 48 h (fresh solution at each period)	Vapor phase	None	Corrosion rate : mpy; mm/y	Solution-annealed; sensitized at 675°C for 1 h; water quenched	Uniform corrosion (higher rate)
			0.02–0.18	Boiling (temperature values not explicitly reported)	240	Periodic renewal every 48 h (fresh solution at each period)	Condensate phase	None	Corrosion rate : mpy; mm/y	Solution-annealed; sensitized at 675°C for 1 h; water quenched	Negligible uniform corrosion
			9 (initial) - varied 8.2–12.2 during boiling	Boiling (temperature values not explicitly reported)	240	Periodic renewal every 48 h (fresh solution at each period)	Renewed liquid phase	0.03 M NaF + 0.15 M $Al(NO_3)_3$ (ratio 5:1)	Corrosion rate : mpy; mm/y	Solution-annealed; sensitized at 675°C for 1 h; water quenched	Uniform corrosion (IGC not observed)
			9	Boiling (temperature values not explicitly reported)	240	Periodic renewal every 48 h (fresh solution at each period)	Vapor phase	0.03 M NaF + 0.15 M $Al(NO_3)_3$ (ratio 5:1)	Corrosion rate : mpy; mm/y	Solution-annealed; sensitized at 675°C for 1 h; water quenched	Uniform corrosion (higher rate)
			9	Boiling (temperature values not explicitly reported)	240	Periodic renewal every 48 h (fresh solution at each period)	Condensate phase	0.03 M NaF + 0.15 M $Al(NO_3)_3$ (ratio 5:1)	Corrosion rate : mpy; mm/y	Solution-annealed; sensitized at 675°C for 1 h; water quenched	Negligible uniform corrosion
(Balbaud et al., 2000)	AISI 304L Stainless Steel	Glass reactor	8	111	1920 (80 days)	Solution renewed every 7 days	Renewed liquid phase	None	Cumulated mass loss : mg·dm^{-2}	Pickled in a fluoronitric bath and passivated in 10% HNO_3 for 14 h	Predominantly uniform corrosion; incipient IGC observed at the end of the test (after 80 days), without grain loss
			8	111	1920 (80 days)	Solution renewed every 7 days	Renewed liquid phase	None	Cumulated mass loss : mg·dm^{-2}	Pickled in a fluoronitric bath and passivated in 10% HNO_3 for 14 h	Predominantly uniform corrosion; incipient IGC observed at the end of the test (after 80 days), without grain loss
			≈ 6	≈ 108	1920 (80 days)	Solution renewed every 7 days	Condensate phase	None	Cumulated mass loss : mg·dm^{-2}	Pickled in a fluoronitric bath and passivated in 10% HNO_3 for 14 h	Severe IGC with grain loss occuring after 43 days
			≈ 6	≈ 108	1920 (80 days)	Solution renewed every 7 days	Condensate phase	None	Cumulated mass loss : mg·dm^{-2}	Pickled in a fluoronitric bath and passivated in 10% HNO_3 for 14 h	Severe IGC with grain loss occuring after 43 days
			8	111	504 (21 d)	Solution renewed every 7 days	Renewed liquid phase	None	Cumulated mass loss : mg·dm^{-2}	Pre-etched in Ce(IV) solution (0.055 mol/L Ce(IV) in 4 mol/L HNO_3) and passivated	Low mass loss observed in the liquid phase on a surface exhibiting pre-existing intergranular features due to pre-etching
			≈ 6	≈ 108	504 (21 d)	Solution renewed every 7 days	Condensate phase	None	Cumulated mass loss : mg·dm^{-2}	Pre-etched in Ce(IV) solution (0.055 mol/L Ce(IV) in 4 mol/L HNO_3) and passivated	Severe IGC with grain loss occuring from the first period of testing
			8	111	1920 (80 days)	Solution renewed every 7 days	Renewed liquid phase	None	Cumulated mass loss : mg·dm^{-2}	Pickled in a fluoronitric bath and passivated in 10% HNO_3 for 14 h (non pre-etched)	Predominantly uniform corrosion; incipient IGC observed at the end of the test (after 80 days), without grain loss
			≈ 6	≈ 108	1920 (80 days)	Solution renewed every 7 days	Condensate phase	None	Cumulated mass loss : mg·dm^{-2}	Pickled in a fluoronitric bath and passivated in 10% HNO_3 for 14 h (non pre-etched)	Severe IGC with grain loss occuring after 43 days
			4 and 8 (liquid immersion only)	Not explicitly reported (same conditions as reference test)	50 d condensate + alternating liquid/condensate	Non-renewed	Alternating liquid/condensate phase	None	Corrosion rate : mg·dm^{-2}·day^{-1}	Pickled in fluoronitric bath and passivated in 10% HNO_3 for 14h	Severe IGC in condensate phase; temporary decrease of corrosion rate upon liquid immersion (4–8 mol·L^{1}), with reactivation upon return to condensate exposure
			≈ 6	≈ 108	Up to 35 days (15 days under NO flow)	Not explicitly reported	Condensate phase	NO, NO_2 , N_2 , 75% O_2 –25% N_2 (gas flow, 1 L·h^{-1})	mg·dm^{-2}	Pickled in fluoronitric bath and passivated in 10% HNO_3 for 14h	Severe IGC in condensate phase under NO flow; no significant effect under N_2, NO_2, or O_2/N_2
		CIRCE loop	Liquid: 8 / Condensate: 4–5	T_{liquid}= 111 ; T_{wall} = 109	up to 60 days	Condensate flow (30 mL·$^{-1}$ in corrosion column)	Condensate phase	None	mg·dm^{-2}	Pickled in fluoronitric bath and passivated in 10% HNO_3 for 14h	Severe IGC (same behavior as test 1)
		CIRCE loop	Condensate: 6	T_{wall} = 110	up to 25 days	Condensate flow (20 mL·h^{-1})	Condensate phase (synthetic)	None	mg·dm^{-2}	Pickled in fluoronitric bath and passivated in 10% HNO_3 for 14h	Severe IGC (similar to natural condensate)
		CIRCE loop	Condensate: 6	T_{wall} = 110	up to 35 days	Condensate flow (20 → 70 → 300 mL·$^{-1}$)	Condensate phase (synthetic)	None	mg·dm^{-2}	Pickled in fluoronitric bath and passivated in 10% HNO_3 for 14h	Severe IGC; corrosion rate decreases with increasing condensate flow rate
		CIRCE loop	Liquid: 8 / Condensate: 4–6	T_{wall} = 108, 109 and 110	up to 60 days	Condensate flow (20, 30 and 40 mL·$^{-1}$)	Condensate phase	None	mg·dm^{-2}	Pickled in fluoronitric bath and passivated in 10% HNO_3 for 14h	Severe IGC; earlier initiation at higher wall temperature
(Coriou et al., 1961)	18/10 austenitic stainless steel, very low carbon (close to 304L composition)	Reactor (boiling acid, reflux condenser)	5	Boiling (110)	Up to 200	Not reported (likely non-renewed)	Liquid phase	Cr(VI) 1 g/L (Potassium dichromate)	Corrosion rate : mg·cm^{-2}·h^{-1}; Cumulated mass loss : mg·cm^{-2}	Degreased, pickled in a fluoronitric bath and passivated in HNO_3	Severe IGC with grain detachment
			5	Boiling (110)	Up to 200	Renewed twice per day (fresh HNO 5 N + Cr(VI) solution)	Liquid phase	Cr(VI) 1 g/L (Potassium dichromate)	Corrosion rate : mg·cm^{-2}·h^{-1}; Cumulated mass loss : mg·cm^{-2}	Degreased, pickled in a fluoronitric bath and passivated in HNO_3	Severe IGC with grain detachment
			5	Boiling (110)	Up to 200	Not reported (likely non-renewed)	Liquid phase	Cr(III) 1 g/L (Chromium nitrate)	Corrosion rate : mg·cm^{-2}·h^{-1}; Cumulated mass loss : mg·cm^{-2}	Degreased, pickled in a fluoronitric bath and passivated in HNO_3	IGC (lower intensity)
			5	Boiling (110)	Up to 200	Not reported (likely non-renewed)	Liquid phase	Cr(VI) 5 g/L (Potassium dichromate)	Corrosion rate : mg·cm^{-2}·h^{-1}; Cumulated mass loss : mg·cm^{-2}	Degreased, pickled in a fluoronitric bath and passivated in HNO_3	Severe IGC (grain detachment)
			11	Boiling (110)	Up to 200	Not reported (likely non-renewed)	Liquid phase	Cr(VI) 1 g/L (Potassium dichromate)	Corrosion rate : mg·cm^{-2}·h^{-1}; Cumulated mass loss : mg·cm^{-2}	Degreased, pickled in a fluoronitric bath and passivated in HNO_3	IGC (initially severe, decreases due to rapid Cr(VI) reduction)
(Badet & Poineau, 2020)	AISI 304L Stainless Steel	PFA immersion cell (ASTM G31-72)	3.5	45	**5 durations** : 4 days, 10 days, 31 days, 92 days, 183 days	Non-renewed	Non-renewed liquid phase	Uranyl nitrate (UN), 0 M	Corrosion rate: µm·y^{-1}	Polished (SiC P400→P4000, diamond 3 µm + 1 µm)	Uniform corrosion; no IGC observed
			3.5	45	**5 durations** : 4 days, 10 days, 31 days, 92 days, 183 days	Non-renewed	Non-renewed liquid phase	Uranyl nitrate (UN), 0.3 M	Corrosion rate: µm·y^{-1}	Polished (SiC P400→P4000, diamond 3 µm + 1 µm)	Uniform corrosion; no IGC observed
			8	45	**5 durations** : 4 days, 10 days, 31 days, 92 days, 183 days	Non-renewed	Non-renewed liquid phase	Uranyl nitrate (UN), 0 M	Corrosion rate: µm·y^{-1}	Polished (SiC P400→P4000, diamond 3 µm + 1 µm)	Uniform corrosion; no IGC observed
			8	45	**5 durations** : 4 days, 10 days, 31 days, 92 days, 183 days	Non-renewed	Non-renewed liquid phase	Uranyl nitrate (UN), 0.3 M	Corrosion rate: µm·y^{-1}	Polished (SiC P400→P4000, diamond 3 µm + 1 µm)	Uniform corrosion; no IGC observed
			3.5	90	**5 durations** : 4 days, 10 days, 31 days, 92 days, 183 days	Non-renewed	Non-renewed liquid phase	Uranyl nitrate (UN), 0 M	Corrosion rate: µm·y^{-1}	Polished (SiC P400→P4000, diamond 3 µm + 1 µm)	Predominantly uniform corrosion; weak IGC after long exposure
			3.5	90	**5 durations** : 4 days, 10 days, 31 days, 92 days, 183 days	Non-renewed	Non-renewed liquid phase	Uranyl nitrate (UN), 0.3 M	Corrosion rate: µm·y^{-1}	Polished (SiC P400→P4000, diamond 3 µm + 1 µm)	Predominantly uniform corrosion; weak IGC after long exposure
			8	90	**5 durations** : 4 days, 10 days, 31 days, 92 days, 183 days	Non-renewed	Non-renewed liquid phase	Uranyl nitrate (UN), 0 M	Corrosion rate: µm·y^{-1}	Polished (SiC P400→P4000, diamond 3 µm + 1 µm)	Severe IGC; grain loss observed between 92–183 days
			8	90	**5 durations** : 4 days, 10 days, 31 days, 92 days, 183 days	Non-renewed	Non-renewed liquid phase	Uranyl nitrate (UN), 0.3 M	Corrosion rate: µm·y^{-1}	Polished (SiC P400→P4000, diamond 3 µm + 1 µm)	Severe IGC; grain loss more pronounced with Uranyl nitrate (UN)
(Yamamoto et al., 1998)	Type 304ULC (Ultra Low Carbon) Stainless Steel	Pyrex boiling-flask immersion system	9	Boiling (≈ 120)	480	Solution renewed every 96 h	Renewed Liquid phase	Ce(IV), 1.0 × 10^{-5} mol/m^3	Corrosion rate: g·m^{-2}h^{-1}	As-received (no specific surface preparation reported)	Severe intergranular corrosion; grain loss observed
			9	Boiling (≈ 120)	480	Solution renewed every 96 h	Renewed Liquid phase	Ce(IV), 1.0 × 10^{-5} mol/m^3 + γ irradiation (4 MR/h)	Corrosion rate : g·m^{-2}h^{-1}	As-received (no specific surface preparation reported)	Intergranular corrosion reduced; fewer grain losses
			9	Boiling (≈ 120)	480	Solution renewed every 96 h	Renewed Liquid phase	Cr(VI), 2.0 × 10^{-5} mol/m^3	Corrosion rate: g·m^{-2}h^{-1}	As-received (no specific surface preparation reported)	Severe IGC with extensive grain detachment
			9	Boiling (≈ 120)	480	Solution renewed every 96 h	Renewed Liquid phase	Cr(VI), 2.0 × 10^{-5} mol/m^3 + γ irradiation (4 MR/h)	Corrosion rate : g·m^{-2}h^{-1}	As-received (no specific surface preparation reported)	IGC still present but significantly moderated
			9	Boiling (≈ 120)	480	Solution renewed every 96 h	Renewed Liquid phase	Ru(III), 4.0 × 10^{-6} mol/m^3	Corrosion rate : g·m^{-2}h^{-1}	As-received (no specific surface preparation reported)	Severe IGC; widespread grain loss
			9	Boiling (≈ 120)	480	Solution renewed every 96 h	Renewed Liquid phase	Ru(III), 4.0 × 10^{-6} mol/m^3 + γ irradiation (4 MR/h)	Corrosion rate : g·m^{-2}h^{-1}	As-received (no specific surface preparation reported)	IGC present; grain loss reduced vs non-irradiated
(Whillock & Dunnett, 2003)	18/13/Nb Stainless Steel	Glass test vessel	8	100	up to 1250 h	Not reported (likely non-renewed)	Liquid phase	Fe(III), 25 g/L	Corrosion rate : mm·y^{-1}	Ground to 800 grit	Severe IGC; grain dropping at steady state
	304L NAG Stainless Steel		9	95	(24 h pre-corrosion + test)	Not reported (likely non-renewed)	Liquid phase	Pre-corrosion: Cr(VI) 1 g/L	Corrosion rate : mm·y^{-1}	Pre-corroded (8M HNO_3 + Cr(VI), 24 h)	IGC with stable grain dropping from start
	Uranus 65 (AISI 310L Stainless Steel)		8	103–105	up to 600 h	Not reported (likely non-renewed)	Liquid phase	Ru(III) 0.7 g/L + Fe(III) 3 g/L	Corrosion rate : mm·y^{-1}	Pre-corroded (Cr(VI) or V method)	Severe IGC; strong anisotropy; end-grain pitting
(Shit & Ningshen, 2019)	Modified AISI 304L Stainless Steel	ASTM A262 practice C apparatus	11.5 (65% wt)	Boiling	240	Solution renewed every 48 h (fresh solution at each cycle)	Renewed liquid phase	None	Corrosion rate : mm·y^{-1}	Wet ground to 1000-grit (SiC)	Predominantly uniform corrosion with increasing IGC features in SEM
(Yamamoto et al., 1996)	AISI 304L Stainless Steel	Pyrex leaching system (boiling nitric acid)	9	Boiling (110°C)	240	Solution renewed every 48 h	Renewed liquid phase	None	Corrosion rate : g·m^{-2}·h^{-1}	Polished to SiC #400	Intergranular corrosion; morphology insensitive to irradiation
(Gwinner et al., 2010)	AISI 304L stainless steel (solution-annealed and quenched; grain size ≈ 45µm)	Immersion setup (continuously renewed solution	8	Boiling (value not explicitly reported)	Exposure durations up to 17 days	Solution renewed continuously	Renewed liquid phase	Ce(IV), 7 g·L^{-1}	Corrosion rate (from groove geometry : Vj, Vs): µm·day^{-1}; thickness loss: µm	No specific surface preparation reported	Severe intergranular corrosion (grooves + grain dropping); morphology used for model validation
(Irisawa & Kato, 2024)	R-SUS304ULC stainless steel	Glass flask with reflux	3	60 (non-boiling)	720	Solution renewed every 240 h	Renewed liquid phase	V(V), Cr(III), Ru, Ce, Fe (very low concentrations)	Corrosion rate: 0.0068 g·m^{-2}·h^{-1} (0.0074 mm·y^{-1})	Polished to SiC #1200	Slight intergranular corrosion (no grain loss)
			8	60 (non-boiling)	720	Solution renewed every 240 h	Renewed liquid phase	Same low metal-ion levels as Case 1	Corrosion rate: 0.020 g·m^{-2}·h^{-1} (0.022 mm·y^{-1})	Polished to SiC #1200	Early intergranular corrosion (minor)
			8	60, 7 kPa (boiling)	720	Solution renewed every 240 h	Renewed liquid phase	Same low metal-ion levels as Case 1	Corrosion rate: 0.14 g·m^{-2}·h^{-1} (0.16 mm·y^{-1})	Polished to SiC #1200	Intergranular corrosion + grain loss visible after 720 h
			8	60, 7 kPa (boiling)	720	Solution renewed every 240 h	Renewed liquid phase	High oxidant levels: V(V), Cr(III), Ru, Ce, Fe	Corrosion rate: 0.30 g·m^{-2}·h^{-1} (0.33 mm·y^{-1})	Polished to SiC #1200	Severe IGC; extensive grain dropping
(Mayuzumi, Ohta, & Arai, 1998)	Type 304L ELC (extra low carbon) Stainless Steel (UNS S30403)	Glass flask	11, 12, 13	Boiling (temperature values not explicity reported)	Up to 1300	Solution renewed every 50–100 h	Renewed liquid phase	None	Accelerating weight loss; constant rate reached after 1000 h	As-machined	Severe IGC with grain shedding at steady state (1000 h)
	Type 310Nb Stainless Steel (UNS S31040)		11, 12, 13	Boiling (temperature values not explicity reported)	Up to 1300	Solution renewed every 50–100 h	Renewed liquid phase	None	Generalized corrosion	As-machined	Uniform corrosion morphology; no grain dropping observed
(Kain, Shinde, & Gadiyar, 1994)	AISI 304L NAG (Nitric Acid Grade) Stainless Steel	ASTM A262 Practice C apparatus (Huey test)	11.5 (65% HNO_3)	Boiling (temperature values not explicity reported)	240	Solution renewed every 48 h	Renewed liquid phase	None	Corrosion rate: 0.152 mm/year (6 mpy)	Not explicitly reported	Uniform corrosion; Low IGC susceptibility (fine grain, retained CW)
			11.5 (65% HNO_3)	Boiling (temperature values not explicity reported)	240	Solution renewed every 48h	Renewed liquid phase	None	Corrosion rate: 0.191 mm·y^{-1}	Not explicitly reported	Still low attack (discontinuous carbides GB)
			11.5 (65% HNO_3)	Boiling (temperature values not explicity reported)	240	Solution renewed every 48h	Renewed liquid phase	None	Corrosion rate: 0.221 mm·y^{-1}	Not explicitly reported	Low corrosion; microstructure stable
			11.5 (65% HNO_3)	Boiling (temperature values not explicity reported)	240	Solution renewed every period	Renewed liquid phase	None	Corrosion rate: 0.223 mm·y^{-1}	Not explicitly reported	Low IGC; resistant microstructure
		End-grain corrosion test	9	Boiling (temperature values not explicity reported)	96	Solution renewed every 24h	Renewed liquid phase	1 g·L^{-1} Cr(VI)	Corrosion rate: 14.48→19.56 mm·y^{-1}	120-grit emery paper	Lower end-grain attack than CP
		IGC test (impurity-segregation)	5	Boiling (temperature values not explicity reported)	33 periods (3 h each)	Solution renewed every 3h	Renewed liquid phase	0.46 N Cr(VI)	Corrosion rate (final): 50.8 mm·y^{-1}	120-grit emery paper	High oxidizing conditions; NAG slightly less attacked
	304L stainless steel (commercial purity)	ASTM A262 Practice C (Huey test)	11.5 (65% HNO_3)	Boiling (temperature values not explicity reported)	240	Solution renewed every 48h	Renewed liquid phase	None	Corrosion rate: 0.305 mm·y^{-1}	Not explicitly reported	IGC susceptibility moderate (AR condition)
			11.5 (65% HNO_3)	Boiling (temperature values not explicity reported)	240	Solution renewed every 48h	Renewed liquid phase	None	Corrosion rate: 0.914 mm·y^{-1}	Not explicitly reported	High IGC susceptibility after sensitization
			11.5 (65% HNO_3)	Boiling (temperature values not explicity reported)	240	Solution renewed every period 48h	Renewed liquid phase	None	Corrosion rate: 1.117 mm·y^{-1}	Not explicitly reported	Severe IGC (continuous precipitation)
			11.5 (65% HNO_3)	Boiling (temperature values not explicity reported)	240	Solution renewed every 48h	Renewed liquid phase	None	Corrosion rate: 1.016 mm·y^{-1}	Not explicitly reported	Severe transgranular + intergranular corrosion
		End-grain corrosion test	9	Boiling (temperature values not explicity reported)	96	Solution renewed every 24h	Renewed liquid phase	1 g·L^{-1} Cr(VI)	Corrosion rate: 9.15→25.91 mm·y^{-1}	120-grit emery paper	Severe end-grain attack
		IGC test (impurity-segregation)	5	Boiling (temperature values not explicity reported)	33 periods (3 h each, last = 4 h)	Solution renewed every 3h	Renewed liquid phase	0.46 mol·L^{-1} Cr(VI)	Corrosion rate (final): 50.8 mm·y^{-1}	120-grit emery paper	Severe IGC (Cr(VI); impurity-driven)
(Sun et al., 2022)	304L stainless steel (solution-annealed)	Self-developed three-phase nitric acid corrosion apparatus (liquid / vapor / condensate compartments)	6	20	120	Not explicitly reported	Liquid phase	Cr(VI) 0.125 g·L^{-1}; V(V) 1.7 g·L^{-1}; Ce(IV) 1.06 g·L^{-1}	Corrosion rate: mm·year^{-1}	2000 SiC + 1.5 µm diamond polish; ultrasonic cleaning	Uniform corrosion (no IGC)
			6	60	120	Not explicitly reported	Liquid phase	Cr(VI) 0.125 g·L^{-1}; V(V) 1.7 g·L^{-1}; Ce(IV) 1.06 g·L^{-1}	Corrosion rate: mm·year^{-1}	2000 SiC + 1.5 µm diamond polish; ultrasonic cleaning	Uniform corrosion (no IGC)
			6	80	120	Not explicitly reported	Liquid phase	Cr(VI) 0.125 g·L^{-1}; V(V) 1.7 g·L^{-1}; Ce(IV) 1.06 g·L^{-1}	Corrosion rate: mm·year^{-1}	2000 SiC + 1.5 µm diamond polish; ultrasonic cleaning	Uniform corrosion (corrosion products visible)
			6	100	120	Not explicitly reported	Liquid phase	Cr(VI) 0.125 g·L^{-1}; V(V) 1.7 g·L^{-1}; Ce(IV) 1.06 g·L^{-1}	Corrosion rate: mm·year^{-1}	2000 SiC + 1.5 µm diamond polish; ultrasonic cleaning	Intergranular corrosion (IGC) present
			6	120	120	Not explicitly reported	Liquid phase	Cr(VI) 0.125 g·L^{-1}; V(V) 1.7 g·L^{-1}; Ce(IV) 1.06 g·L^{-1}	Corrosion rate: mm·year^{-1}	2000 SiC + 1.5 µm diamond polish; ultrasonic cleaning	Intergranular corrosion (IGC) present
			Not explicitly reported	60	120	Not explicitly reported	Vapor phase	None	Corrosion rate: mm·year^{-1}	2000 SiC + 1.5 µm diamond polish; ultrasonic cleaning	Uniform corrosion (no IGC)
			Not explicitly reported	80	120	Not explicitly reported	Vapor phase	None	Corrosion rate: mm·year^{-1}	2000 SiC + 1.5 µm diamond polish; ultrasonic cleaning	Uniform corrosion (no IGC)
			Not explicitly reported	100	120	Not explicitly reported	Vapor phase	None	Corrosion rate: mm·year^{-1}	2000 SiC + 1.5 µm diamond polish; ultrasonic cleaning	Uniform corrosion (no IGC)
			Not explicitly reported	120	120	Not explicity reported	Vapor phase	None	Corrosion rate: mm·year^{-1}	2000 SiC + 1.5 µm diamond polish; ultrasonic cleaning	Uniform corrosion (no IGC)
			Not explicitly reported	60	120	Not explicitly reported	Condensate phase	None	Corrosion rate: mm·year^{-1}	2000 SiC + 1.5 µm diamond polish; ultrasonic cleaning	Uniform corrosion (no IGC)
			Not explicitly reported	80	120	Not explicitly reported	Condensate phase	None	Corrosion rate: mm·year^{-1}	2000 SiC + 1.5 µm diamond polish; ultrasonic cleaning	Uniform corrosion (no IGC)
			Not explicitly reported	100	120	Not explicitly reported	Condensate phase	None	Corrosion rate : mm·year^{-1}	2000 SiC + 1.5 µm diamond polish; ultrasonic cleaning	Uniform corrosion (no IGC)
			Not explicitly reported	120	120	Not explicitly reported	Condensate phase	None	Corrosion rate: mm·year^{-1}	2000 SiC + 1.5 µm diamond polish; ultrasonic cleaning	Uniform corrosion (no IGC)
(Mudali et al., 1993)	304L stainless steel (commercial grade)	Boiling nitric acid reflux setup with condenser (ASTM Practice C–type)	65 wt.% (≈ 15.5 M)	Boiling	240	Renewed every 48 h	Renewed liquid phase	None	mm·year^{-1}	Polished to 600 grit SiC	Severe intergranular corrosion, grain dropping, tunnel (end-grain) corrosion
	304L NAG (Nitric Acid Grade) stainless steel		65 wt.% (≈ 15.5 M)	Boiling	240	Renewed every 48 h	Renewed liquid phase	None	mm·year^{-1}	Polished to 600 grit SiC	Grain-boundary grooving, partial grain spalling; lower attack than commercial 304L
	Uranus 16 stainless steel (304L NAG , extra-low carbon, low impurities)		65 wt.% (≈ 15.5 M)	Boiling	240	Renewed every 48 h	Renewed liquid phase	None	mm·year^{-1}	Polished to 600 grit SiC	Minimal intergranular corrosion; no tunnel corrosion; highly stable oxide layer
	Uranus 65 stainless steel (NAG 310L, high-Cr, low impurities)		65 wt.% (≈ 15.5 M)	Boiling	240	Renewed every 48 h	Renewed liquid phase	None	mm·year^{-1}	Polished to 600 grit SiC	Very low corrosion; excellent resistance comparable to Zircaloy-2